Electronic Supplementary Material (ESI) for RSC Advances.

Supplementary Information

Mesoporous nickel phosphate/phosphonate hybrid microspheres with excellent performance for adsorption and catalysis

Yun-Pei Zhu,[a] Ya-Lu Liu,[a] Tie-Zhen Ren[b] and Zhong-Yong Yuan[a,*]

[a] *Key Laboratory of Advanced Energy Materials Chemistry (Ministry of Education), Collaborative Innovation Center of Chemical Science and Engineering (Tianjin), College of Chemistry, Nankai University, Tianjin 300071, China. E-mail: zyyuan@nankai.edu.cn*

[b] *School of Chemical Engineering & Technology, Hebei University of Technology, Tianjin 300130, China.*

Experimental Section

Materials. $NiCl_2$, $Ni(NO_3)_2$, $NiSO_4$, Na_2HPO_4, NaH_2PO_4, Na_3PO_4, sodium borohydride ($NaBH_4$), and 4-nitrophenol were obtained from Tianjin Kermel Chemical Co. $Cu(NO_3)_2$, $Pb(NO_3)_2$ and $Cd(NO_3)_2$ were purchased from Tianjin Guanggu Chemical Co. Ethylene diamine tetra(methylene phosphonic acid) (EDTMP, Fig. S1) 1-hydroxyethane-1,1-diphosphonic acid (HEDP, Fig. S1), and bis-(hexamethylenetriamine)-penta(methylenephosphonic acid) (BHMTPMP, Fig. S1) was donated from Henan Qingyuan Chemical Co. All chemicals were used as received without further purification.

Preparation of the Nickel Phosphate/Phosphonate Microspheres. Typically, 10 ml of 0.4 mol L^{-1} $NiCl_2$ solution was dropwise added into 20 ml of 0.05 mol L^{-1} H_3PO_4 aqueous solution under vigorous stirring, followed by the addition of 4 mmol EDTMP, and the final pH was kept around 5. After 2 h of stirring, the obtained mixture was transferred into a Teflon-lined autoclave and aged statically at 180 ºC under autogenous pressure for 36 h. The as-synthesized green products were filtered, washed by distilled water and ethanol alternatively for several times, and dried at 120 ºC overnight. The final sample was marked as NiPPH, abbreviated for nickel phosphate/phosphonate hybrid.

Measurements and Characterization. Scanning electron microscopy (SEM) was carried out on a Jeol JSF-7500L at 5 keV. Transmission electron microscopy (TEM) was carried out on a Jeol JEM 2100F at 200 kV. All samples subjected to TEM measurements were ultrasonically dispersed in ethanol and dropcast onto copper grids covered with a carbon film. X-ray diffraction (XRD) patterns were recorded on a Bruker D8 Focus Diffractometer with Cu-Kα radiation (λ = 0.15418 nm) operated at 40 kV and 40 mA. N_2 adsorption-desorption isotherms were measured on a Quantachrome NOVA 2000e sorption analyzer at liquid nitrogen temperature (77 K). The samples were degassed at 120 ºC overnight prior to the measurement. The surface areas were calculated by the multi-point Brunauer-Emmett-Teller (BET)

method, the pore size distributions were obtained from the adsorption branch of the isotherms by the NLDFT (Non-local Density Functional Theory) model. Fourier transform infrared (FT-IR) spectra were measured on a Bruker VECTOR 22 spectrometer with KBr pellet technique, and the ranges of spectrograms were 4000 to 400 cm^{-1}. Diffuse reflectance UV-vis. absorption spectroscopy was employed on a Shimadzu UV-2450 UV-vis spectrophotometer. Simultaneous thermogravimetry (TG) and differential scanning calorimetry (DSC) were performed using a TA SDT Q600 instrument at a heating rate of 5 ºC/min using α-Al_2O_3 as the reference. X-ray photoelectron spectroscopy (XPS) measurements were performed on a Kratos Axis Ultra DLD (delay line detector) spectrometer equipped with a monochromatic Al-Kα X-ray source (1486.6 eV). All XPS spectra were recorded using an aperture slot of 300 × 700 microns, survey spectra were recorded with a pass energy of 160 eV, and high resolution spectra with a pass energy of 40 eV.

CO_2 Capture Measurements. The CO_2 adsorption isotherms of the materials were measured on a Quantachrome Autosorb-1 MP analyzer at 0 and 25 ºC. Each sample was outgassed for 12 h at 120 ºC to remove the guest molecules from the pores before starting the adsorption measurements and then cooled down to room temperature, followed by the introduction of CO_2 into the system. To investigate the reusability of NiPPH for capturing CO_2, after the adsorption was reached, the sample was degassed again at 120 ºC for 12 h to remove the adsorbed CO_2 molecules completely before the next CO_2 capture test.

Metal Ions Adsorption. The potential of NiPPH for the adsorption of different analyzing ions (Pb^{2+}, Cu^{2+}, and Cd^{2+}) was tested as follows: 0.02 g of the samples were added into 10 ml metal nitrides aqueous solutions with different concentrations (0.02 – 0.4 × 10^{-4} mol/L). The mixture was stirring for 6 hours to access the adsorption-desorption balance, followed by centrifugation at 6000 rpm for 15 min. The concentrations of metal ions in the initial and final solutions were monitored through atomic absorption spectroscopy (AAS) analysis. The maximal adsorption capacity was calculated by the Langmuir model using the equation $n_s = Kn_mc/(1 + Kc)$, where K is the Langmuir constant, c is the metal ion concentration,

n_m is the monolayer adsorption capacity, and n_s is the amount of metal ion adsorbed on the adsorbent. To test the reusability of the NiPPH for chelating heavy metal ions, the Pb^{2+} ions loaded sample was taken as representative and treated with 1 mol L^{-1} hydrochloric acid for 6 h to remove the metal ions, and then neutralized, following a second round adsorption test (0.05×10^{-4} mol L^{-1} of Pb^{2+}).

Catalytic Activity Test. The reduction of 4-NP was carried out under ambient condition. To a 15 ml of 1.33 mmol L^{-1} 4-NP solution, 5 ml of 1.6 mol L^{-1} $NaBH_4$ catalyst and 0.02 g of NiPPH were added under stirring. The molar ratio of $n(NaBH_4)$: n(4-NP) is 400. The blank experiment was taken out in the absence of any catalysts. For comparison purpose, the reaction was carried out in the presence of pure EDTMP. The catalytic hydrogenation of 4-NP is commonly of second order. When the concentration of $NaBH_4$ is in large excess with the respect to that of 4-NP, this reaction could thus be considered as pseudo first order reaction, of which the reaction rate is independent from the $NaBH_4$. The 4-NP solution shows light yellow that then turns to bright yellow as the addition of $NaBH_4$, which is due to the formation of phenolate ions presenting a strong adsorption peak at 400 nm.[1] So the catalytic activity can be evaluated by detecting the variation of the adsorption at 400 nm using a UV-vis spectrometer (Shimadzu UV-2450). Since the amount of $NaBH_4$ is in a large excess, the reduction reaction can be regarded as a pseudo first-order reaction based on the evaluation of the rate constant with regard to 4-NP only: $\ln(C_0/C) = kt$, where C_0 and C are the concentrations of 4-NP at time t and 0, respectively, k is the rate constant (min^{-1}), t is the reaction time.

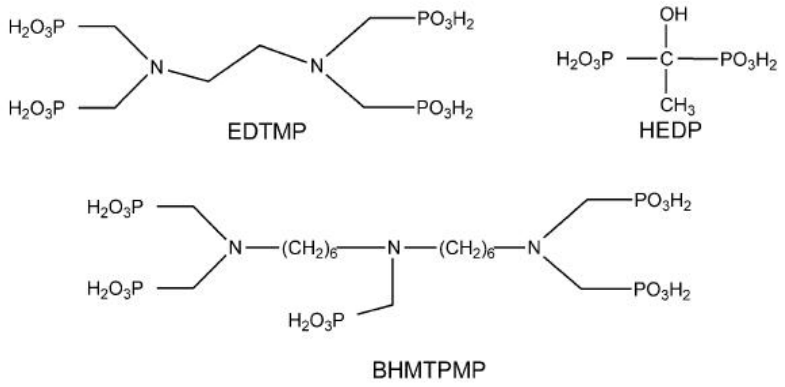

Fig. S1 Structural formula of EDTMP, HEDP and BHMTPMP.

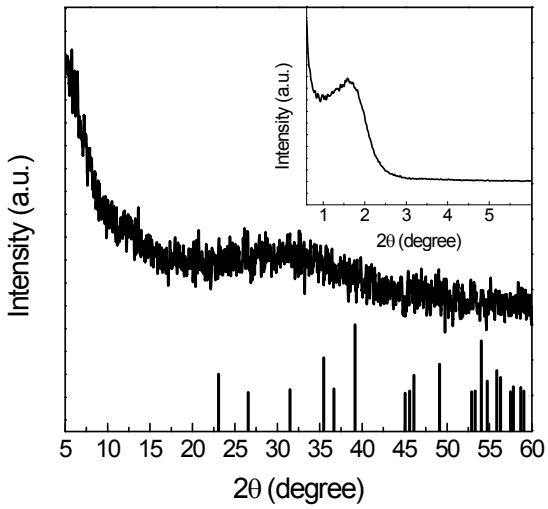

Fig. S2 Wide-angle XRD patterns of the NiPPH hybrid, the vertical black lines show the standard diffractions of nickel phosphate (JCPDS No. 38-1473). Inset: low-angle diffraction patterns.

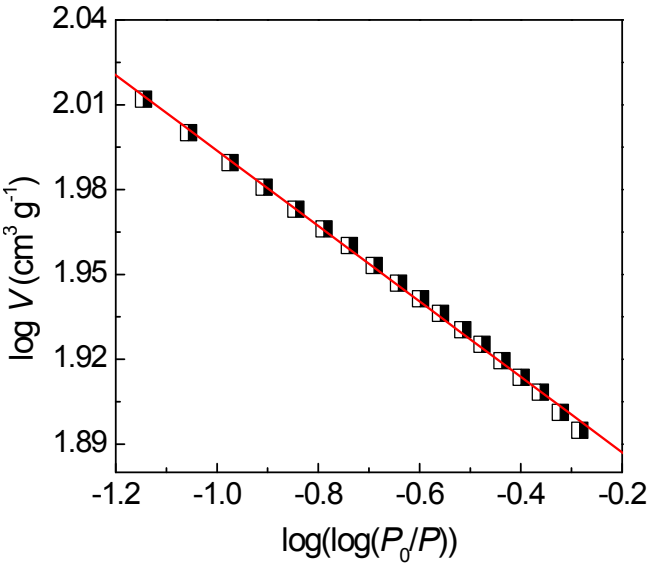

Fig. S3 FHH isotherm of the NiPPH sample.

Fractal analysis from the nitrogen adsorption isotherms was employed to investigate the pore surface roughness of the synthesized hybrid microspheres in terms of surface fractal dimension (*D*). The *D* value ranges from 2 for perfectly smooth surfaces to 3 for sponge-like surfaces, and the degree of surface irregularity increases with the increase of the fractal dimension.[2,3] The surface fractal dimension according to Frenkel-Halsey-Hill (FHH) model yields the follow formula:[4]

$$V = k[\log(P_0/P)]^{D-3}$$

D value can be calculated from the slope of a plot of log*V* versus log(log(P_0/*P*)):

$$\log V = (D\text{-}3)\ \log(\log(P_0/P))$$

where *k* is a material constant, *P* and P_0 are the equilibrium and saturation pressures of nitrogen adsorbed, and *V* represents of the nitrogen adsorbed volume at a given pressure *P*. Noticeably, the FHH model is valid in the multilayer regime but not capable of monolayer adsorption (low pressure region) and capillary condensation (high pressure region). The plot of ln*V* versus log(log(P_0/*P*)) can be well linearly fitted in the relative pressure range from 0.3 to 0.85, resulting in a correlation coefficient (R^2) of 0.9992. The fractal dimension can thus be determined to be 2.866.

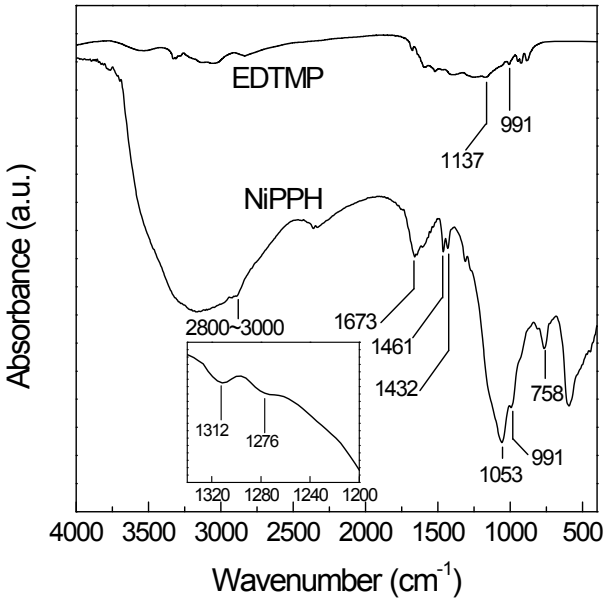

Fig. S4 FT-IR spectra of pristine EDTMP coupling molecule and the NiPPH material.

A shoulder vibration band at 991 cm^{-1} is attributed to P–OH and the band at 1053 cm^{-1} can be assigned to P–O···Ni vibrations. The band at 1137 cm^{-1} ascribed to P=O stretching vibration in the phosphonate groups is not observed in NiPPH, which implies the connection of P=O to Ni atoms. A weak shoulder at 1276 cm^{-1} stems from the asymmetric stretching vibration of O–P–O groups of the phosphate,[5] and the signal at 758 cm^{-1} suggests the presence of P-O-P bending modes.[6] The overlapped bands at 1461 and 1432 cm^{-1} are assigned as the C–H bending in $–CH_2–$ groups and the P–C stretching vibrations, respectively. Weak bands around 2800–3000 cm^{-1} are assigned to the C–H stretching modes. The small weak bands at 1312 cm^{-1} can be attributed to C–N stretching. The strong, broad band at 3400 cm^{-1} and the sharp band at 1673 cm^{-1} correspond to the surface-adsorbed water and hydroxyl groups.

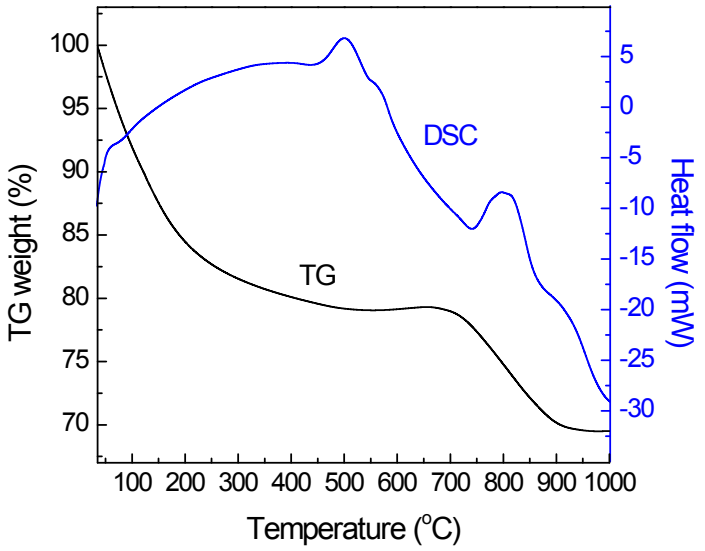

Fig. S5 TG-DSC curves of the NiPPH material.

The thermal stability of the nickel phosphate-phosphonate hybrid was determined by TG–DSC analysis. The initial weight loss of 15.4 % from room temperature to 190 ºC can be attributed to the desorption of the adsorbed and intercalated water. The TG curve also demonstrates a weight loss in the range of 190 – 950 ºC, accompanied with two main exothermal peaks at 503 and 802 ºC in the corresponding DSC curve, which can be related to the decomposition and combustion of the organic phosphonate components in the hybrid framework.

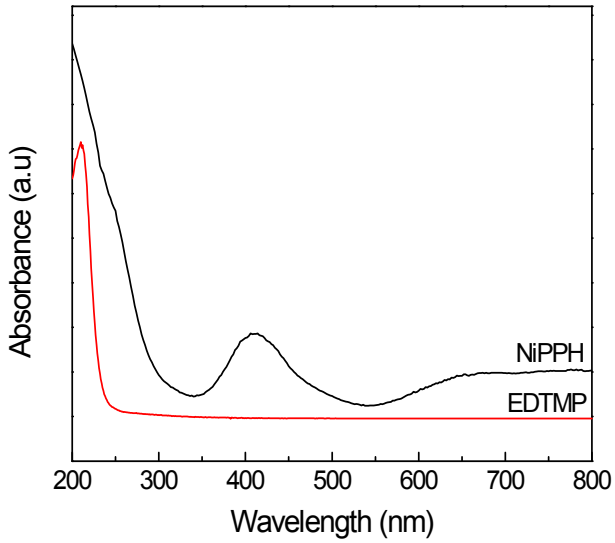

Fig. S6 UV-vis. absorption spectrum of EDTMP and the NiPPH hybrid.

The pristine phosphonic precursor shows single strong adsorption in UV region having a sharp absorption peak situating at 210 nm. This kind of absorbance character has been well retained in the NiPPH material to a considerable extent. Furthermore, for the NiPPH material, it exhibits one major absorption band in the visible spectrum with maximum at 411 nm attributed to the electronic transition from O^{2-} 2p to Ni^{2+} 3d orbital and the other broad absorption in the wavelength range of 550 – 800 nm. The high energy absorption band for this hybrid nickel phosphate/phosphonate indicates that the octahedral coordination of Ni is dominant and the phosphonic linkages is present in the hybrid network.[7,8]

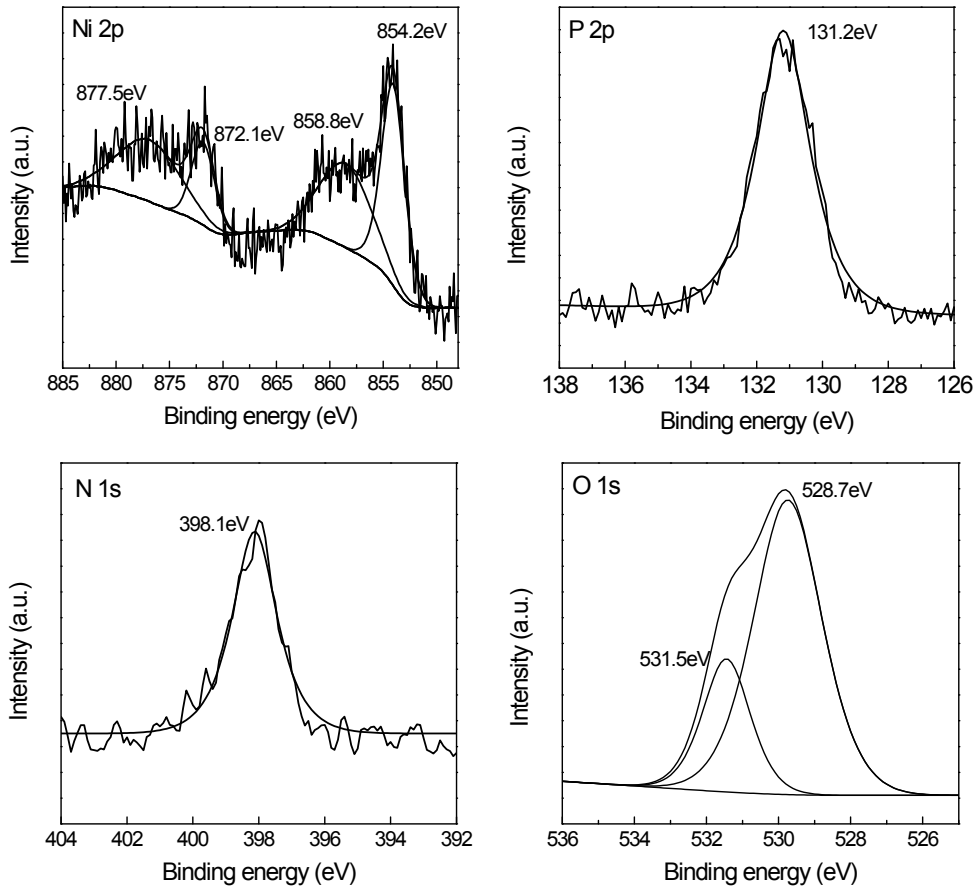

Fig. S7 High-resolution XPS spectrum of Ni 2p, P2p, N 1s, and O1s of NiPPH.

The Ni 2p line is rather complicated and can be deconvoluted into four components. The Ni $2p_{3/2}$ and Ni $2p_{1/2}$ peaks positioned at about 854.2 eV and 872.1 eV, with the corresponding satellite peaks at 858.8 and 877.5 eV, respectively, which indicates that the nickel element exists in the form of Ni^{2+} in the organic-inorganic hybrid. The P 2p spectrum exhibits a peak at 131.2 eV, which is the characteristic of P^{5+} contributing from the phosphonate and phosphate groups. A single peak at 398.1 eV for N 1s spectrum, corresponding to the N atoms in the phosphonate bridging components, can be observed. Curve-fitting the high resolution O 1s spectrum suggests that there should be two kinds of oxygen. The main signals at 528.7 eV is assigned to the oxygen in the P–O···Ni linkage, while the shoulder around 531.7 eV are ascribed to the oxygen from the surface hydroxyl and defective P–OH.

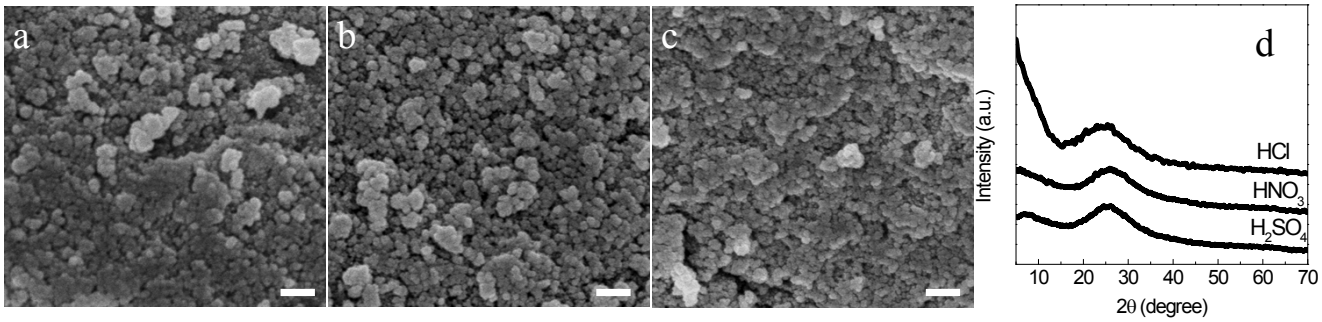

Fig. S8 SEM images of nickel phosphonate hybrids synthesized in the presence of HCl (a), HNO_3 (b), and H_2SO_4 (c), respectively, scale bar: 200 nm. (d) gives the corresponding XRD patterns, no crystalline diffractions corresponding to nickel phosphate could be observed.

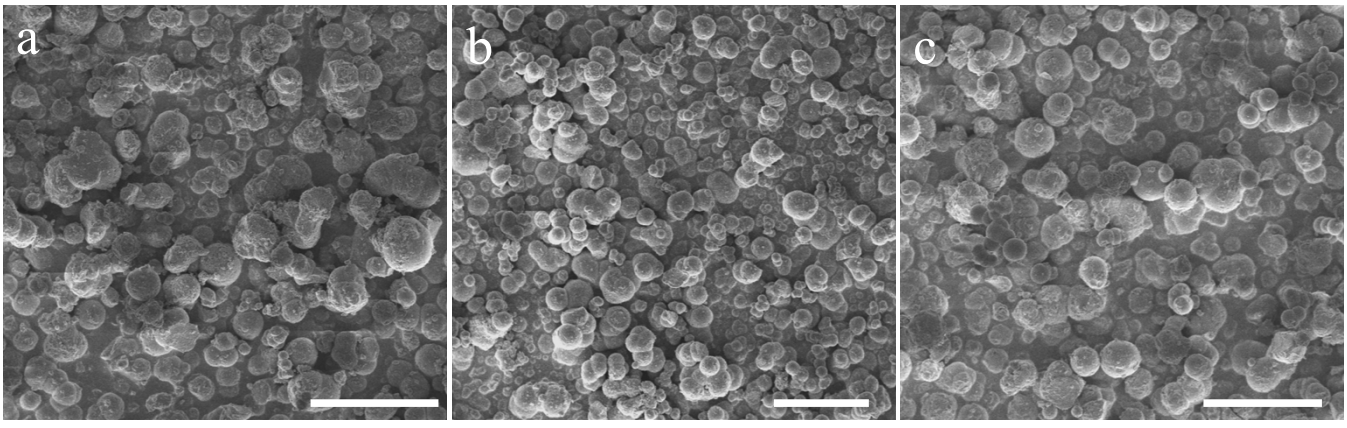

Fig. S9 SEM images of nickel phosphate/phosphonate hybrids synthesized with NaH_2PO_4 (a), Na_2HPO_4 (b), and Na_3PO_4 (c) used as phosphoric sources, respectively. Scale bar: 10 μm.

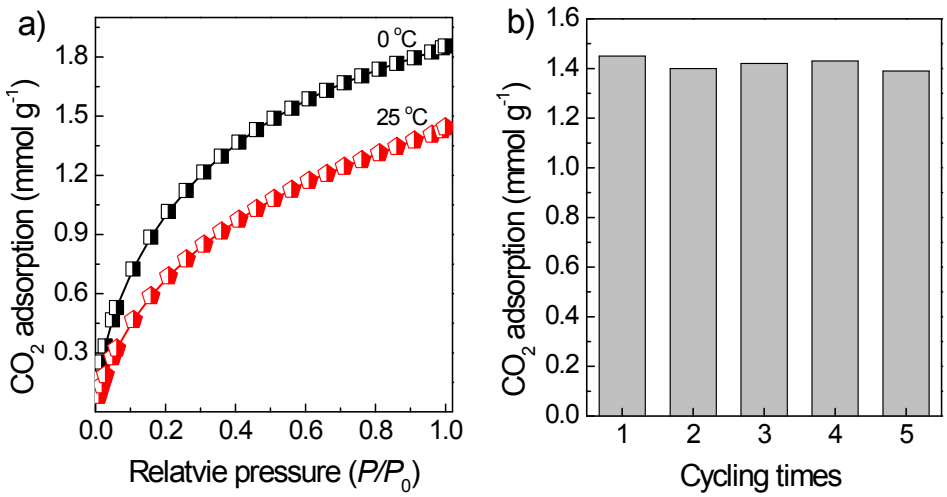

Fig. S10 (a) CO_2 adsorption isotherms of NiPPH at 0 and 25 ºC and (b) reusability of the adsorbent measured at 25 ºC.

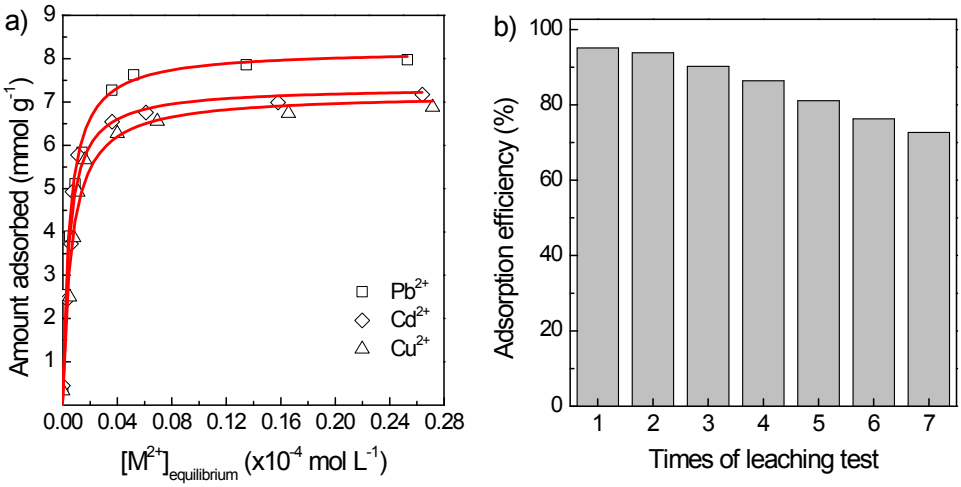

Fig. S11 (a) Adsorption isotherms of the NiPPH material for the removal of heavy metal ions and the red solid lines were the simulated lines using Langmuir equation. (b) Reusability of the adsorbents for seven cycles.

The multiple adsorption results show that the Pb^{2+} uptake capacity remains more than 90.0 % after three times use. Then adsorption capacity decreased gradually in the next successive uses, but the materials still retain greater than 70 % of the original adsorption efficiency after leaching seven times. During multiple leaching tests, the Pb^{2+} residues could be retained and so occupy the coordination sites for further adsorption or transform into PbO or $Pb(OH)_2$ species, which could block the pore channels. The superposition of these effects would lead to the decrease of the adsorption efficiency.

References

1 K. Hayakawa, T. Yoshimura and K. Esumi, *Langmuir*, 2003, **19**, 5517−5521.

2 Q. Wei and D. Wang, *Mater. Lett.*, 2003, **57**, 2015−2020.

3 W. Xu, T. W. Zerda, H. Yang and M. Gerspacher, *Carbon*, 1996, **34**, 165−171.

4 A. Du, B. Zhou, W. W. Xu, Q. J. Yu, Y. Shen, Z. H. Zhang and J. Shen, G. M. Wu, *Langmuir*, 2013, **29**, 11208−11216.

5 M. Abid, M. Et-tabirou and M. Hafid, *Mater. Res. Bull.*, 2001, **36**, 407−421.

6 T. Y. Ma and Z. Y. Yuan, *Dalton Trans.*, 2010, **39**, 9570−9578.

7 B. A. Breeze, M. Shanmugam, F. Tuna and R. E. P. Winpenny, *Chem. Commun.*, 2007, 5185−5187.

8 V. Baskar, M. Shanmugam, E. C. Sañudo, M. Shanmugam, D. Collison, E. J. L. McInnes, Q. Wei and R. E. P. Winpenny, *Chem. Commun.*, 2007, 37−39.